Journal of **large-scale** **research** facilities

Journal of large-scale research facilities, 10, A192 (2026) http://dx.doi.org/10.17815/jlsrf-10-192

Published: 14.07.2026

The Ludwieg Tube Wind Tunnel Göttingen (RWG)

German Aerospace Center (DLR)
Institute of Aerodynamics and Flow Technology *

Instrument Scientists:
- E. Schülein, Erich.Schülein@dlr.de
- J. Lunte, Jens.Lunte@dlr.de
- W. Lühder, Wieland.Lühder@dlr.de
- A. Wagner, Alexander.Wagner@dlr.de

Abstract: The Ludwieg Tube Wind Tunnel Göttingen (RWG) of the German Aerospace Centre (DLR) has been operating successfully since 1968 and is the world's first intermittently operating large-scale aerodynamic research facility based on the Ludwieg tube principle. This wind tunnel principle was originally developed by Hubert Ludwieg for the cost-effective experimental investigation of supersonic and hypersonic flows at high Reynolds numbers. Intermittent operation ensures that the required operating power and costs remain moderate, even at high flow rates. The RWG is still the largest research facility of its kind in Europe. It has two storage tubes 80 m long and six supersonic nozzles covering discrete Mach numbers from 2 to 7. The test section diameter is 0.5 m (or 0.5 m × 0.5 m) and test times are up to 320-380 ms. The facility is ideal not only for the validation of new numerical methods, but also for the study of complex phenomena in supersonic and hypersonic flows. The effects of the transition from laminar to turbulent flow and the interactions between shock waves and the boundary layer, e.g. on the aerothermal loads of re-entry or high-speed vehicles, can be studied in detail.

*Cite article as: **Cite article as:** German Aerospace Center (DLR). (2026). The Ludwieg Tube Wind Tunnel Göttingen (RWG). *Journal of large-scale research facilities, 10*, A192. http://dx.doi.org/10.17815/jlsrf-10-192

1 Introduction

2 The working principle of a Ludwieg tube wind tunnel

The Ludwieg tube concept was developed in the mid-1950s by Professor Hubert Ludwieg at the Aerodynamische Versuchsanstalt Göttingen (AVA). For a detailed description of how a Ludwieg tube works, please refer to the work of the inventor and his colleagues Ludwieg (1955); Ludwieg et al. (1969). The following is a brief overview of the most important details necessary to understand the function of the individual components of the facility.
The unique design of a Ludwieg tube, with its pressure reservoir in the form of a long tube, ensures that the flow parameters (total pressure, total temperature) remain almost constant over the test time. This is achieved without the need for additional control devices. Figure 1 shows the scheme of a Ludwieg tube, according to Ludwieg et al. (1969). The pressure vessel consists of a long storage tube (a) closed at one end and fitted with a quick-acting gate valve (b) at the other end. This is followed by a supersonic nozzle (c), the test section with model support (d) and the dump tank (f). When the valve opens, a packet of expansion waves travels towards the closed end of the tube at the local speed of sound, creating a flow. These waves are reflected when they reach the closed end and return. While these waves have not yet reached the nozzle throat, test gas continues to flow through the nozzle and test section into the dump tank, maintaining nearly constant stagnation conditions. Figure 2 from the cited paper further illustrates the process described using a simplified path-time diagram of the flow in the storage tube and nozzle from the moment the valve opens to the end of the measurement time.

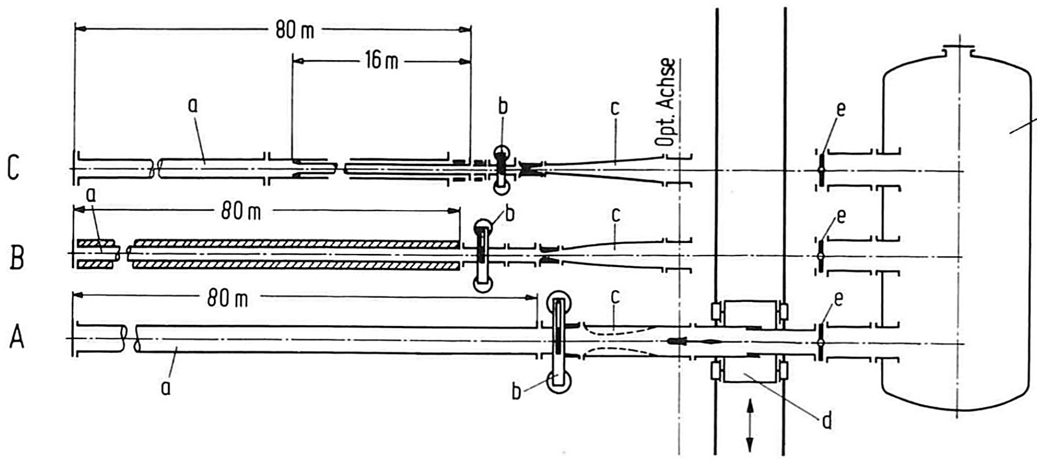

Figure 1: Sketch of the RWG from Ludwieg et al. (1969).

RWG and the High Enthalpy Shock Tunnel Göttingen (HEG, (Deutsches Zentrum für Luft- und Raumfahrt (DLR), 2024)) at the Göttingen site enable a complementary and synergistic use: RWG supports validation at lower enthalpies with long-duration, high-quality flow conditions, while HEG provides access to high-enthalpy flight regimes.

2.1 Description of the RWG

Figure 3 shows the typical time histories of total pressure and total temperature over two first test periods, measured in the storage tube immediately upstream of the quick-opening valve at Mach 6 flow conditions. The start of the measurement time is defined by the initial drop in total pressure. However, a closer look reveals that the passage of the expansion waves is accompanied by a brief increase in the resulting total pressure (re-compression) about 10-15 ms after the start of valve opening (see also Figure 2). This is due to the supercritical taper of the tube cross-section inside the Laval nozzle. The initial acceleration of the air at the valve opening is greater than the contraction of the

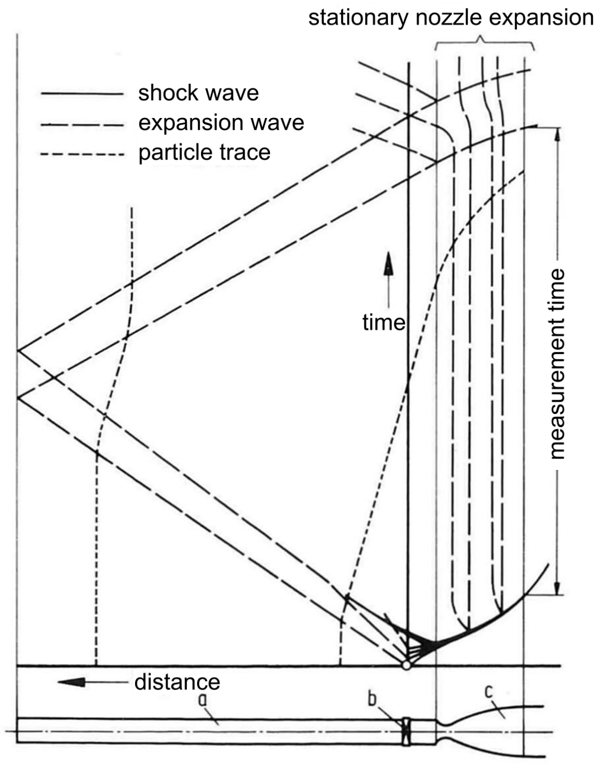

Figure 2: Simplified path-time diagram of the flow in the storage tube and nozzle from Ludwieg et al. (1969).

nozzle contour, allowing it to pass through the nozzle throat unhindered (Kantrowitz limit). This creates compression waves in the converging part of the nozzle, weakening the traveling expansion waves and thus adjusting the mean Mach number of the pipe flow. Only when this has happened (at about 25-30 ms) does the expected quasi-stationary flow state occur and the Mach number, total pressure and total temperature in the storage tube remain almost constant until the reflected expansion waves arrive (at about 340 ms). The expansion waves then reflect at the convergent part of the nozzle and travel back into the storage tube. The second test period begins at approximately 410 ms, when the flow parameters have stabilized at the new level, and continues until the expansion waves return to the nozzle inlet (at approximately 720 ms). Strictly speaking, the flow parameters do not really remain constant during these test periods. A slight and systematic drop in P_0 during this time can be explained by the viscosity related losses in the pipe flow and is directly visible in the plots. Due to the limited temporal resolution, the total temperature variations shown are significantly less reliable than those of the total pressure. The challenge of reliably measuring temperature variations is well known in all short-duration wind tunnels, since the thermocouples must be sufficiently robust to withstand the dynamic loads during operation. Unfortunately, such thermocouples are unable to follow the rapid temperature changes during the start up process.

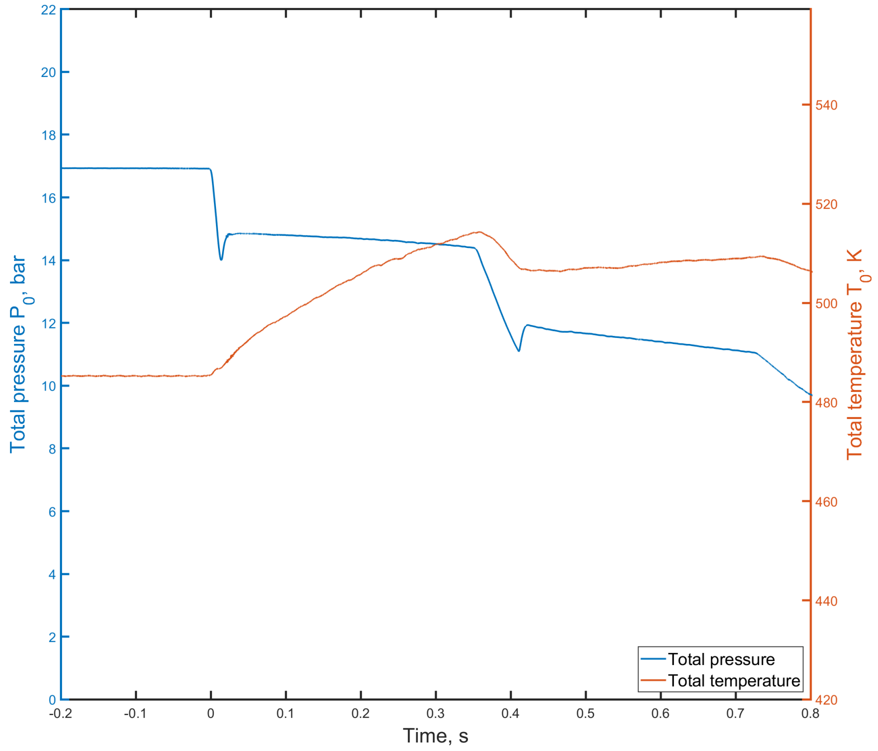

Figure 3: Typical time histories of total pressure and total temperature in storage tube of RWG at Mach 6 test conditions.

2.1.1 RWG test conditions

The RWG currently covers a Mach number range of $2 \leq M_\infty \leq 7$ and an unit Reynolds number range of $2 \times 10^6\ \mathrm{m}^{-1} \leq Re_\infty \leq 11 \times 10^7\ \mathrm{m}^{-1}$. The range of test conditions in the facility is documented in the table 1. The variations in total temperature shown for the unheated tube A (M_∞ = 2, 3 and 4) roughly correspond to the expected variation in ambient temperature, taking into account the energy input from filling the storage tube with compressed air. Unfortunately, it is not possible to set this temperature exactly. The lowest total flow temperatures that can actually be achieved in the heated tube B (M_∞ = 5, 6 and 6.85) correspond to the re-sublimation limit of nitrogen and are strictly dependent on the static pressure around the test model. For this reason the T_0 and maximum Re_∞ values given in this table should be taken as a guide only.

Table 1: Flow parameter range of the RWG

Tube	A	A	A	B	B	B
Ma	2	3	4	5	6	6.85
p_0, MPa	0.05-0.7	0.06-0.6	0.08-1.0	0.4-2.9	0.4-3.4	0.4-3.6
T_0, K	236-262	241-267	258-287	340-610	410-640	440-655
Re_∞, $10^6\,\mathrm{m}^{-1}$	10-110	6-70	4-60	5-60	3-33	2-20
Test section	0.34 × 0.35 m^2	0.5 × 0.5 m^2	0.5 × 0.5 m^2	⌀0.5 m	⌀0.5 m	⌀0.5 m

2.1.2 RWG storage tubes

The RWG is currently equipped with only two storage tubes, designated A and B. The third storage tube C, shown in Fig. 1, which was originally designed for Mach numbers greater than 7, was decommissioned in the late 1990s due to technical problems. Tube A for Mach numbers 2, 3 and 4 has an internal diameter of 339 mm. It is unheated and designed for a maximum charge pressure of 15 bar. Tube B for Mach numbers 5, 6 and 7 has an internal diameter of 150 mm. It can be heated to 400°C and charged to 40 bar. The smaller the tube diameter, the greater the influence of the boundary layer on the flow. To counteract this, the air velocity in the tube is kept lower than in tube A and the inner wall of the tube is honed to a roughness depth of no more than 20 μm to achieve the smoothest possible surface.

2.1.3 Heating device

The storage tube B is heated as an ohmic resistance via rectifiers. A total of two heating rectifiers with a voltage range of 0 to 22 V at 3000 A are connected in series. With the power installed, the tubes can be heated to maximum temperature in approximately two hours. As the tube is thermally insulated, this temperature can then be maintained with significantly reduced power.

2.1.4 RWG quick opening valves

The available time for measurement is not only reduced by the start-up process described above, but also by the effective opening time of the valve. To address this, particular emphasis was placed on the selection and configuration of the high-speed valves during the planning and construction phases of the facility. Quick opening gate valves are located between the storage tube and the nozzle and are opened and closed by compressed air. The two fast gate valves used at the RWG have opening times of approximately 50-60 ms (tube A, $M_\infty \leq 4$) and 15-20 ms (tube B, $M_\infty \geq 5$). The opening time of the fast gate valve and the resulting Mach number of the quasi-stationary tube flow after start-up can be reliably estimated from the time history of the Pitot pressure in the storage tube. The opening diameter of the valve plate is exactly the same as the internal diameter of the storage tube. By closing the valves at the end of the measurement time, a large proportion of the stored air is retained in the storage tube and unnecessary filling of the vacuum vessel is avoided. This also reduces operating costs and allows a longer measurement sequence. The nominal test time of the RWG, specified as the time required for the reflected expansion waves to reach the nozzle again after the valve is opened, is approx. 320-380 ms. As this is only dependent on the temperature of the compressed air for a given length of storage tube, the longer test times correspond to a cold tube A.

2.1.5 RWG nozzles

The cross-sectional ratio of nozzle throat to test section changes from 0.5930 at M_∞ = 2 to 0.0106 at M_∞ = 6.85, with several individual nozzles assigned to each storage tube. Contoured flat nozzles are used at tube A, only contoured axially symmetric nozzles are used at tube B. With the exception of the Mach 2 nozzle, the outlet dimensions of these nozzles are always the same and are 500×500 mm^2 (M_∞ = 3 and 4) or 500 mm in diameter (M_∞ = 5, 6 and 6.85). The Mach 2 nozzle was built later and has a reduced outlet area of 340×350 mm^2 to keep the tube Mach number within limits. All nozzles have a 300 mm diameter window at the test section location for model observation. All supersonic nozzles for higher Mach numbers have been in use since the facility was commissioned, with the exception of the Mach 3 nozzle, which was completely redesigned in the late 1990s.

2.1.6 RWG model support and dump tank

There is an adjustable model support in the connection between the nozzle and the dump tank, to which the model support stings are attached. This device allows the angle of attack to be changed from -15° to

+15° with respect to the wind tunnel axis. The tube connector is telescopic. By retracting it, the model and holder can be taken out of the test section. The same test section and telescope assembly can be used in combination with all nozzles which simplifies switching the Mach number between tube A and B, as it eliminates the need to remove or re-install the model or change electrical connections.
The dump tank has a volume of 48 m^3 and has been connected to a *COBRA NX* dry screw vacuum pump from Busch Vacuum Solutions since 2021. With the help of this new vacuum pump, the dump tank is evacuated to the desired pressure of around 30-50 mbar in just 15-20 minutes before the facility is started up. This is twice as fast as the previous rotary vane pump. These shorter running times and the electronic speed control of the pump have a very positive effect on the energy consumption of the facility. Using the standard experimental procedure—which includes heating the storage tube, evacuating the dump tank, and setting up the model—up to 16 test runs can be carried out during a standard workday.

3 Measurement Techniques Overview

3.1 High-speed shadowgraphy

High-quality schlieren and shadowgraph visualization techniques are available as standard for visualizing the flow topology on wind-tunnel models. The optical components are arranged in a conventional Z-configuration. A *Cavilux Smart* (400 W) diode laser from *Cavitar Ltd.* is currently used as the short-duration light source; it typically operates in pulsed mode at 2 kHz with a pulse width of 20 ns. A *pco.dimax HS4* camera from *PCO AG* is generally employed for imaging. This camera can record full-resolution images of 2000×2000 pixels at frame rates of up to 2277 fps. The extremely short exposure time allows the system to record high-resolution shadowgraph sequences with essentially no motion blur (see Touré & Schülein (2020)).

3.2 Quantitative Infrared Thermography (QIRT)

Quantitative infrared thermography is now the standard method used in our wind tunnel to measure heat flux density distributions on the model surface. This technique has been used successfully for over 20 years and has proven to be highly reliable (see Schülein (2006); Schülein (2014)). A thick-walled model made of a material with low thermal conductivity is best for determining heat flux density. Assuming a semi-infinite wall thickness, the heat flux density can be calculated if the temporal path of the model surface temperature distribution during the wind tunnel run has been recorded with sufficient accuracy. For a semi-infinite plate abruptly exposed to a heat flux density, q_w, at time t_0, Cook and Felderman's established numerical integration method is used to solve the partial Fourier differential equation and determine the heat flux at each time, t_n:

$$\dot{q}_w(t_n) = 2\sqrt{\frac{\rho_m c_m \lambda_m}{\pi}} \left[\sum_{i=1}^{n} \frac{T_i - T_{i-1}}{\sqrt{t_n - t_i} + \sqrt{t_n - t_{i-1}}} \right] \tag{1}$$

T_{i-1}, T_i and T_n are the surface temperatures at different times t_{i-1}, t_i and t_n; ρ_m, c_m and λ_m are the density, the specific heat capacity and the thermal conductivity of the slab material.
Typically a special insert of the test model is fabricated from black *PLEXIGLAS* or *PEEK*. The time history of the surface temperature is recorded during the wind-tunnel run by the high-resolution infrared camera system *IRCAM EQUUS 327kL pro* at a frame rate up to 105 Hz and an exposure time of 100 μs. This camera is based on a 640×512 FPA-sensor, which is sensitive in the spectral range of 8.0 to 9.4 μm. Optical access to the test section in the Ludwieg tube facility is provided through a custom-build anti-reflection-coated Germanium window. The entire measurement setup is calibrated using a precision blackbody heat-emitter positioned in the test section; this yields the actual transmission coefficients of the IR-window. The surface emissivity ε of the model-insert material is measured indirectly by assuming that ε = 1 - (reflectivity). For this purpose the same blackbody heat-emitter was used to

supply different background temperatures at a known model-wall temperature during the calibration tests.

The recorded temperature fields are processed using the in-house software *HeatFIT*, which enables rapid calculation and visualization of heat-flux distributions immediately after each test run. HeatFIT performs an automatic, marker-based 3D reconstruction of the thermal images and re-projects the results onto the CAD surface of the model, allowing accurate heat-flux evaluation from image sequences acquired from multiple viewing angles. A complete 3D reconstruction is essential for most test models because taking large-area infrared images from a short distance results in noticeable optical distortion. If applicable, markings outside the edges of the inserts enable precise identification of their location within each captured image. Assigning the actual model coordinates to each pixel enables spatial averaging of the heat flux. In two-dimensional flows, for example, averaging can be performed perpendicular to the flow direction to obtain a reliable, reproducible heat flux distribution along that direction. Figure 4 shows a representative infrared image on the left and a nondimensionalized heat flux (Stanton number) distribution on the right. Both were extracted from the full sequence of infrared images recorded.

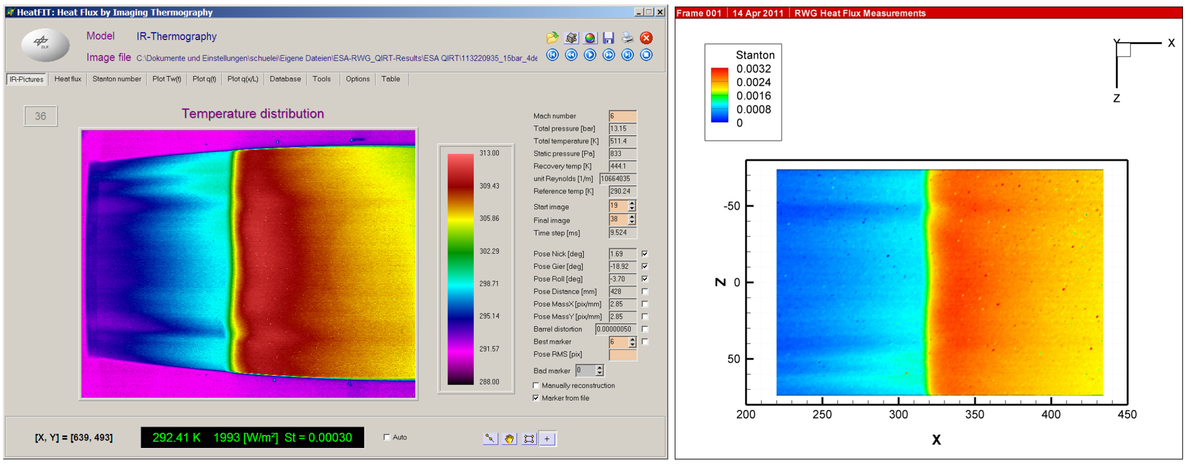

Figure 4: Typical infrared image (left) and corresponding heat-flux distribution (right) derived from an image sequence of a flat-plate model in the RWG, showing the region of shock-wave impingement at Mach 6, with flow from the left.

3.3 Aerodynamic Force and Moment Measurements

Direct measurements of aerodynamic forces and moments in short test time facilities, such as the RWG, present several challenges and require bespoke measurement and evaluation methods. In addition to the measurement errors typically associated with conventional wind tunnels, at least two other issues arise from the sudden onset of airflow.

The most significant of these is the strong oscillations of the model at the suspension rod caused by the propagating shock wave that spreads out from the storage tube towards the test model after the quick-acting valve is opened, before supersonic flow is established in the test section. This initial shock wave acts like a hammer blow on the model and the sting, causing the model to oscillate on the balance. Although these interference vibrations decay, inertial effects can still distort the measurement signals throughout the entire measurement period. Wind tunnel models are too complex and diverse for a simplified damped harmonic oscillator model to reliably extract the desired quasi-stationary force and moment components from dynamic signals. At best, this model can be used to verify the plausibility of the extracted data by recreating the dynamic data. Figures 5 and 6 show some typical paths of the angle of attack, normal force and pitching moment signals for a generic hypersonic model over the two measurement periods of the RWG. Thanks to its long test duration, the Ludwieg tube offers an-

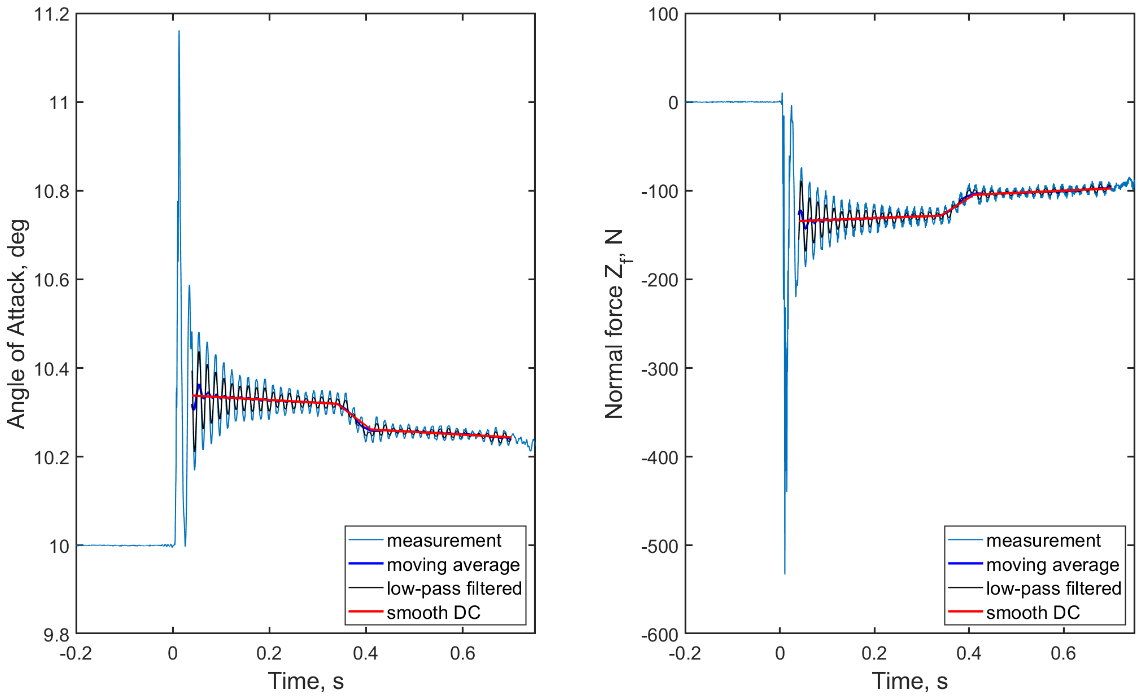

Figure 5: Histories of the angle of attack (left) and normal force (right) for a generic hypersonic model at Mach 6.

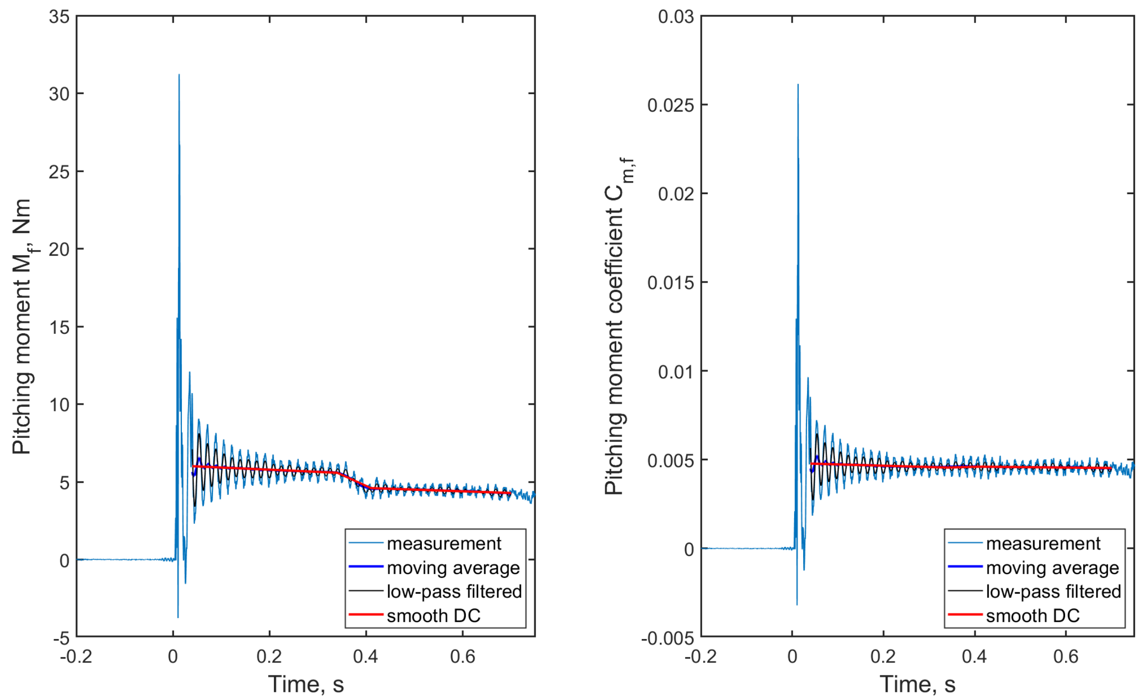

Figure 6: Histories of the pitching moment (left) and pitching moment coefficient (right) for a generic hypersonic model at Mach 6.

other chance to validate the force measurement data. When the observation window extends beyond two measurement periods, it becomes apparent that the model vibrations decay almost completely. The force and moment coefficients determined during this time are quasi-stationary and easily reproducible (see Fig. 6). Therefore, as the oscillations gradually decay, the plausibility of reconstructing the stationary coefficients from the measured dynamic forces and moments can be effectively validated. The high reliability and reproducibility of the extracted force coefficients can be seen in Fig. 7. The diagrams present the final results, using drag and lift coefficients determined from four independent experiments with variations in the Reynolds number as an example. However, based on these results, the actual effect of the Reynolds number cannot yet be clearly separated from the effect of the angle of attack (i.e., the balance deflection caused by the intrinsic change in dynamic pressure associated with variations in the Reynolds number). To achieve this separation, further independent tests are required.

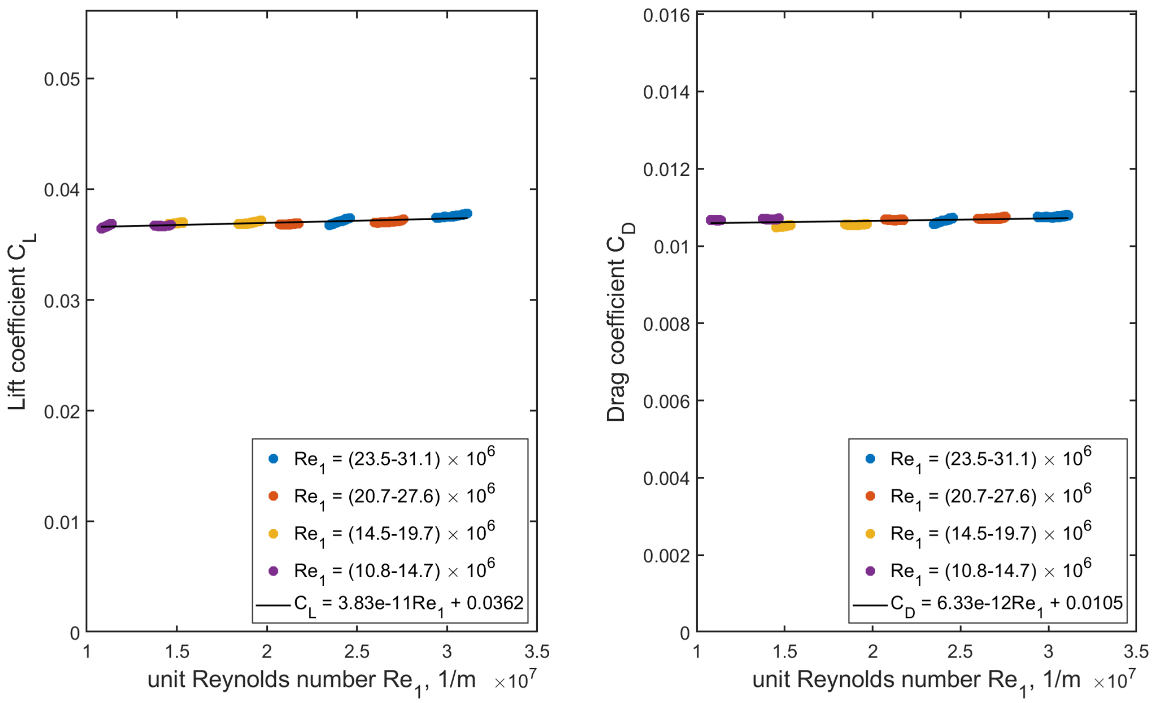

Figure 7: Dependence of the drag and lift coefficients on the unit Reynolds number at Mach 6 from four independent experiments in the RWG.

Another issue affecting force measurements in short-term facilities is the sudden onset of airflow, which results in sustained pressure differences within the balance. To avoid this error, the balance should be open. The model balance used in the RWG has a ventilation slot and a central opening on the back to prevent pressure differences during monotonous parameter changes. However, since these errors cannot be entirely eliminated at the start of the test, force measurement signals are only considered once the flow in the test section has been stable for 40–50 ms.

3.4 Oil film interferometry (OFI)

Oil film interferometry (OFI) is a method to optically measure the wall shear stress on the model surface by observing the motion of a thin oil film (see Lunte & Schülein (2020)). Even though the ideas of this technique exist for nearly 50 years, it has not found general and popular use yet due to complicated and time consuming evaluation steps. The local change in oil film height depends on the wall shear

stress, local surface pressure gradients, gravity and surface tension and can be calculated by the *thin oil-film equation* from Squire (1962). All effects except for the skin friction are neglected in most use cases, which can be justified for very thin oil films with a height of $h \leq 2$ μm. During an experimental campaign, several images are required for the final data evaluation. It is necessary to calculate the photogrammetric matching between 2D image and virtual 3D evaluation grid, to obtain the required vector field of oil flow direction and the oil film height at two distinct points in time needs to be measured.
To achieve this, the model is illuminated by a 0.6×0.6 m^2 diffuse 3 color LED light panel outside of the test section window. This light is reflected by the model surface, where both mirror polished steel surfaces and application of a highly glossy PVC foil have been successfully used. The camera *IO Industries Flare 48M30ccx* is mounted on the same side of the wind tunnel and continuously captures RGB images of the interference pattern at 32 fps and a resolution of 6656$\times$5128 pixels. Any pair of images can be used to calculate the average wall shear stress and thereby skin friction coefficient within the respective time frame.

3.5 Focused Laser Differential Interferometry (FLDI)

Focused Laser Differential Interferometry (FLDI) became an established tool for measuring density differences in supersonic flows over the last decade. Due to its frequency bandwidth of over 1 MHz and the non-invasive detection of density fluctuations, FLDI is used to investigate turbulent dynamics and instabilities in the laminar-turbulent transition (Lunte & Schülein, 2024). The center piece of each FLDI setup is the beam splitting optical element. At the RWG two Wollaston prism (WP) pairs with a separation angle of 2° and 2′ are available. The two Wollaston prism pairs enable the variation of the separation distance between the focal points to optimize for the wave length of interest or can be used to set up a multi-point FLDI system.
The optical setup of the FLDI system is sketched in Fig. 8 and uses a *OBIS 660LX* laser with a wave length of 660 nm as a light source. To condition the beam the laser is focused through a 50 μm pinhole (PH) to create a well-defined focus point and then trimmed by an iris (I) to match the 1-inch aperture of the WP. A linear polarization filter (LPF) before the first WP balances the intensity of both partial beams. A field lens (L) focuses both partial beams at the measurement plane. Afterwards the beams are refocused by a second lens, recombined by a second WP and brought to interference by a second LPF. The interference intensity due to the optical path difference Δs_{opt} is converted to a voltage signal by a photo diode (PD, Thorlabs DETA36A2) and can be digitized by a data acquisition system.

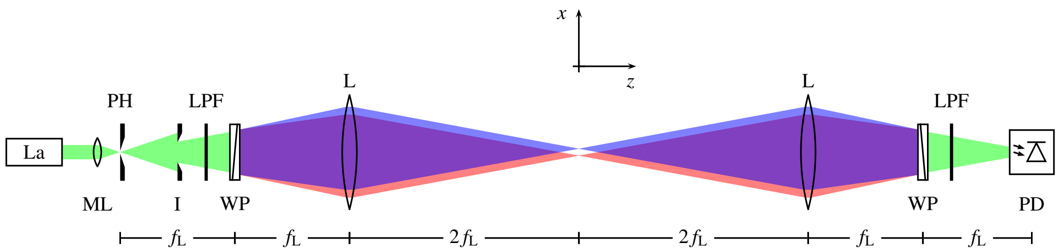

Figure 8: Sketch of the FLDI setup. The separated beams are depicted in blue and red. Overlapping regions are violet (Lunte & Schülein, 2024).

4 Flow quality

The objective of each ground test wind tunnel facility is to generate a homogeneous flow with a freestream turbulence identical to the real flight situation for ideal replication. However, in conventional supersonic wind tunnel facilities, the radiated acoustic waves from the turbulent nozzle wall boundary layer generate freestream fluctuations, which are typically 1 to 2 orders of magnitude above flight conditions (Schneider, 2008). As the freestream noise has a dramatic impact on the laminar-turbulent transition (Schneider, 2001), all experimental ground test data has to be extrapolated to the flight conditions.

For the realization of a tunnel-to-flight extrapolation and for numerical recalculations of wind tunnel results, precise knowledge of the freestream characteristics is required. Here, knowledge of only the general noise level by for example the RMS value of the Pitot pressure is insufficient. Instead, the frequency-dependent amplitude distribution of the fluctuations is necessary (Wagner et al., 2018). The detailed measurement of freestream characteristics has been practiced at the RWG for decades and expanded continuously.

Recently, FLDI was used to investigate the density fluctuations in the freestream of the Mach 6 nozzle at various unit Reynolds numbers Re_1 (Lunte & Schülein, 2024). The measured power spectral densities (PSD) are shown in Fig. 9. A normalization of the measurement signal with the freestream density yields nearly self similar PSD spectra for the Re_1 range, suggesting a systematic behavior of Re_1 on the laminar-turbulent transition, which should be meaningfully reproducible by correlations.

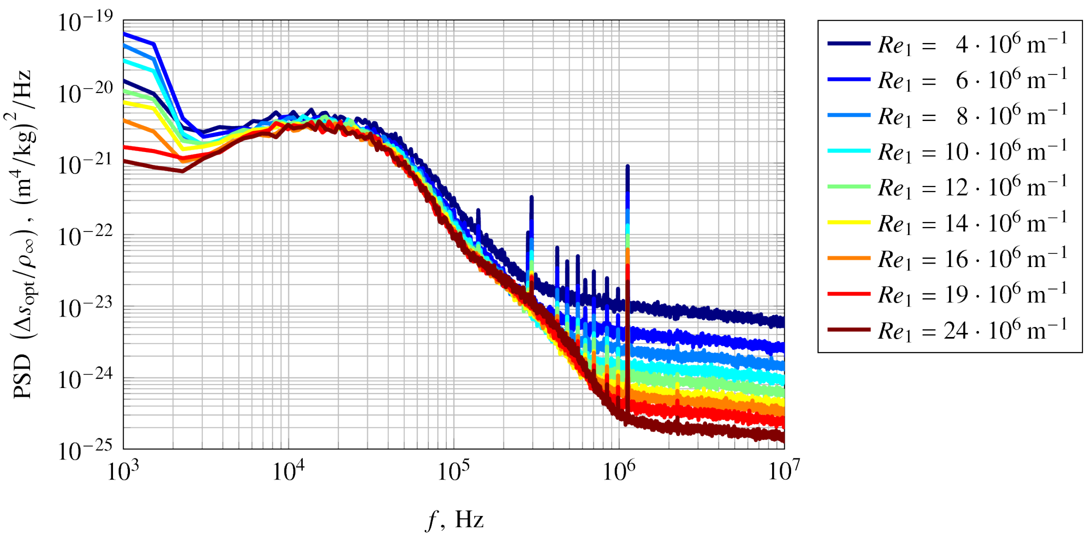

Figure 9: PSD of the freestream density fluctuations at various Re_1 in the RWG Mach 6 nozzle measured by FLDI and scaled by the freestream density (Lunte & Schülein, 2024).

The impact of Re_1 regarding the transition locations on wind tunnel models, was studied at the Mach 6 nozzle a flat plate by QIRT (Schülein, 2014). The transition Reynolds number Re_{tr}, determined by the location of the Stanton number peak, was plotted over Re_1 and compared to the established Ross correlation (Ross, 1972) (see Fig. 10). The agreement of the experimental data with the Ross correlation verifies the plausibility of the RWG results regarding existing concepts about the behaviour of freestream noise in conventional supersonic wind tunnel facilities and its impact on the laminar-turbulent transition.

5 Selected scientific studies

The variety of implemented measurement techniques at the RWG forms the basis for the scientific investigations of scaled flight vehicles and diverse flow phenomena, including SBLI, laminar-turbulent

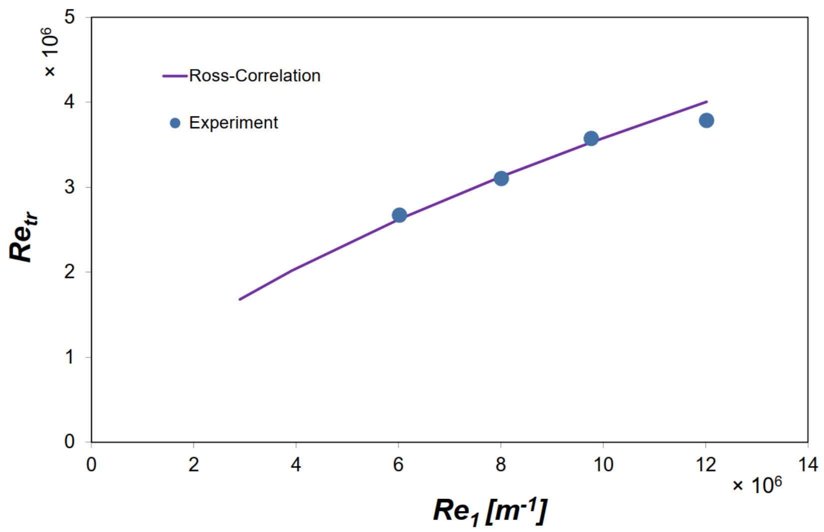

Figure 10: Unit Reynolds number effect on the transitional Reynolds number on a flat plate with a sharp leading edge at Mach 6 in the RWG (Schülein, 2014)

boundary layer transition as well as the maturation of innovative flow optimization concepts. Selected research results are briefly presented below to illustrate the range of past and current activities at RWG. Our facility has a long-standing tradition of supporting European spaceflight programs. During the 1980s and 1990s, the facility made significant contributions through extensive experimental campaigns for the HERMES and SÄNGER projects, supporting the development of aerodynamic databases for hypersonic gliders. Within the framework of the ESA/NASA cooperation on the X-38 Crew Return/Rescue Vehicle (CRV) project, RWG also conducted intensive investigations during this period. Building on these studies, separated flows in the flap region of the X-38 were analyzed both experimentally and numerically in (Lüdeke et al., 2004, 2000), with particular emphasis on heat loads downstream of reattachment induced by streamwise vortices.

To enable a detailed investigation of this phenomenon, large-scale longitudinal vortices in high-speed turbulent separated flows were studied in the RWG Ludwieg tube facility (Schülein & Trofimov, 2007, 2011). These vortices were found to be triggered by relatively small surface irregularities located either at the model leading edge or on the model surface. Wind tunnel experiments were conducted at Mach numbers of 3 and 5, employing oil-flow visualization and infrared thermography to investigate nominally two-dimensional ramp flows at deflection angles of 20°, 25°, and 30°.

Surface contour anomalies were artificially introduced using very thin strips (vortex generators) of varying shapes and thicknesses attached to the model surface. The results showed that the induced streamwise vortical disturbances persist over very large downstream distances—on the order of 10^4 vortex-generator heights—in turbulent supersonic flows without pressure gradients. Furthermore, it was demonstrated that each vortex pair observed in the reattachment region originates from an upstream vortex pair, generated for instance by small roughness elements near the leading edge.

The dependence of the spacing and intensity of the longitudinal vortices on both the characteristics of the imposed disturbances (such as thickness and spanwise extent of the vortex generators) and key flow parameters (including Reynolds number, boundary-layer thickness, and compression corner angle) was systematically established through experimental investigations.

The effect of boundary-layer suction on delaying laminar-turbulent transition on a supersonic swept wing was investigated experimentally at Mach 2 in the RWG within the EU-funded *SUPERTRAC* project (Schülein, 2008). Experiments were conducted for swept-wing configurations with 20° and 30° sweep at unit Reynolds numbers of up to $30 \times 10^6\,\mathrm{m}^{-1}$, with suction velocities varied up to approximately $1.0\,\mathrm{m/s}$. Transition behavior was assessed using oil-film interferometry, quantitative infrared thermography, oil-flow visualization, and supporting wall-pressure and heat-flux measurements. The results show a clear and substantial transition delay due to suction, with particularly strong laminar-flow control for the 30° sweep, where transition Reynolds numbers increased by up to 300%. For the 20° sweep, a moderate but consistent transition delay was observed. Possible contamination of downstream transition data by three-dimensional shock reflections from tunnel walls was identified, limiting transition assessment beyond mid-chord.

The effects of steady and unsteady upstream energy deposition (ED) on hypersonic flow were investigated experimentally using a low-voltage DC arc discharge as well as laser-induced single- and double-pulse optical discharges ahead of conically nosed and spherically blunted bodies at Mach numbers of 2 and 5 (Schülein & Zheltovodov, 2011; Schülein et al., 2010). Experiments conducted in a Ludwieg tube facility combined drag force measurements (steady ED only) with shadowgraph visualization to quantify flow-field modifications caused by localized heating. The interaction between the heated wake and the bow shock, as well as the influence of heating power and body geometry on bow-shock strength, were systematically examined. The results reveal an optimum heating rate that maximizes the effectiveness of energy addition, yielding drag reductions of up to 70% depending on test conditions and model geometry.

The effect of a uniformly moving impinging shock wave on shock-wave/turbulent-boundary-layer interaction was investigated in a combined experimental and numerical study at a free-stream Mach number of 3 (Touré & Schülein, 2020; Touré & Schülein, 2023). While quasi-steady inflow conditions were maintained, the relative Mach number of the travelling shock was varied to isolate the influence of shock motion. The experimental program formed the core of the study and employed a flat-plate configuration with interchangeable stationary and movable shock generators. High-speed shadowgraphy was used to track the shock motion and to determine the interaction length under moving-shock conditions. The experimental data enabled a refinement of an established quasi-steady scaling law by improved modelling of Reynolds number and wall-temperature effects. The resulting scaling accurately predicts interaction lengths for both quasi-stationary and uniformly travelling shock waves, demonstrating the applicability of an extended quasi-steady framework.

The concave bump concept (Lunte & Schülein, 2025a; Schülein et al., 2022) introduces a passive flow control concept to optimize impinging SBLI by methodically spreading the shock-induced pressure rise over an extended distance through a suitable wall deformation, thereby preventing flow separation. Experimental validation using both 2D-planar and axisymmetric wind tunnel models across Mach 3 and 5 conditions confirmed the flow separation suppression at the design point. The wall pressure distributions matched theoretical predictions and CFD simulations demonstrated a halving of the total pressure losses by the SBLI.

The validated freestream flow quality at RWG qualifies the facility for studies on laminar-turbulent boundary layer transition - a critical topic in supersonic flows due to its direct impact on accurate thermal load prediction. To assess the reliability of experimental transition data, three independent measurement techniques—QIRT, PCB pressure sensors, and FLDI— were applied on a Mach 6 flat plate to determine the intermittency distributions (Lunte & Schülein, 2025b). Despite qualitative agreement, the 50 %-intermittency location varied by up to 9.3 % in streamwise Reynolds number, highlighting that multi-method validation is essential for reliable transition characterization, as each technique captures different aspects of the transition process with distinct sensitivities and limitations.

References

Deutsches Zentrum für Luft- und Raumfahrt (DLR). (2024). The high enthalpy shock tunnel göttingen of the german aerospace center (dlr). *Journal of Large-Scale Research Facilities*, *9*, A188. Retrieved from http://dx.doi.org/10.17815/jlsrf-9-1881 http://dx.doi.org/10.17815/jlsrf-9-1881

Ludwieg, H. (1955). Der Rohrwindkanal. *Zeitschrift für Flugwissenschaften*(3), 206–216.

Ludwieg, H., Hottner, T., & Grauer-Carstensen, H. (1969). Der Rohrwindkanal der Aerodynamischen Versuchsanstalt Göttingen. *Jahrbuch 1969 der DGLR*.

Lunte, J., & Schülein, E. (2020). Wall shear stress measurements by white-light oil-film interferometry. *Exp. Fluids*, *61*(84). http://dx.doi.org/10.1007/s00348-020-2917-9

Lunte, J., & Schülein, E. (2024, April). Wall-normal focused laser differential interferometry. *AIAA Journal*, *62*(4), 1366–1374. http://dx.doi.org/10.2514/1.j063258

Lunte, J., & Schülein, E. (2025a). Flow separation control by a concave bump. *EUCASS 2025-308, 11TH EUROPEAN CONFERENCE FOR AERONAUTICS AND SPACE SCIENCES (EUCASS)*. http://dx.doi.org/10.13009/EUCASS2025-308

Lunte, J., & Schülein, E. (2025b). Transition phenomena and intermittency on a mach 6 flat plate evaluated by three independent flow parameters. *Exp. Fluids*, *66*(133). http://dx.doi.org/10.1007/s00348-025-04034-9

Lüdeke, H., Radespiel, R., & Schülein, E. (2004). Simulation of streamwise vortices at the flaps of re-entry vehicles. *Aerospace Science and Technology*, *8*(8), 703–714.

Lüdeke, H., Schülein, E., Radespiel, R., Longo, J. M. A., & Cao, C. Y. (2000). *Reduction of aerothermal uncertainties at turbulent flaps* (Tech. Rep. No. TET-DLR-21-TN-3302). Braunschweig, Germany: DLR.

Ross, R. (1972). A simple formula for flat plate boundary-layer transition in supersonic wind tunnels. *AIAA Journal*, *10*(3), 336–337. http://dx.doi.org/10.2514/3.6585

Schneider, S. P. (2001). Effects of high-speed tunnel noise on laminar-turbulent transition. *Journal of Spacecraft and Rockets*, *38*(3), 323–333. http://dx.doi.org/10.2514/2.3705

Schneider, S. P. (2008). Development of hypersonic quiet tunnels. *Journal of Spacecraft and Rockets*, *45*(4), 641–664. http://dx.doi.org/10.2514/1.34489

Schülein, E. (2006). Skin friction and heat flux measurements in shock/boundary layer interaction flows. *AIAA Journal*, *44*(8), 1732-1741. Retrieved from https://doi.org/10.2514/1.15110 http://dx.doi.org/10.2514/1.15110

Schülein, E. (2008). Experimental investigation of laminar flow control on a supersonic swept wing by suction. *AIAA 2008-4208, 4th Flow Control Conference*, 1-14. Retrieved from https://arc.aiaa.org/doi/abs/10.2514/6.2008-4208 http://dx.doi.org/10.2514/6.2008-4208

Schülein, E. (2014, jun). Effects of laminar-turbulent transition on the shock-wave/boundary-layer interaction. *AIAA 2014-3332, 44th AIAA Fluid Dynamics Conference*. http://dx.doi.org/10.2514/6.2014-3332

Schülein, E., Schnepf, C., & Weiss, S. (2022). Concave bump for impinging-shock control in supersonic flows. *AIAA Journal*, *60*(5), 2749-2766. Retrieved from https://doi.org/10.2514/1.J060799 http://dx.doi.org/10.2514/1.J060799

Schülein, E., & Zheltovodov, A. (2011). Effects of steady flow heating by arc discharge upstream of non-slender bodies. *Shock Waves*, *Vol. 21*(4), 383–396. Retrieved from https://elib.dlr.de/57047/ (Published online: 26 February 2011) http://dx.doi.org/10.1007/s00193-011-0307-1

Schülein, E., Zheltovodov, A. A., Pimonov, E. A., & Loginov, M. S. (2010, September). Experimental and numerical modeling of the bow shock interaction with pulse-heated air bubbles. *International Journal of Aerospace Innovations*, *Vol. 2*(3), 165–188. Retrieved from https://elib.dlr.de/60425/ http://dx.doi.org/10.1260/1757-2258.2.3.165

Schülein, E., & Trofimov, V. (2007). Steady longitudinal vortices in separated turbulent flows. In *Proceedings of the 1st ceas european air and space congress* (pp. 251–260). Berlin, Germany. (CEAS Paper 2007-116, ISSN 0700-4083, 10–13 September 2007)

Schülein, E., & Trofimov, V. (2011). Steady longitudinal vortices in supersonic turbulent separated flows. *Journal of Fluid Mechanics*, *672*, 451–476. http://dx.doi.org/10.1017/S0022112010006105

Squire, L. (1962). The motion of a thin oil sheet under the steady boundary layer on a body. *Flow visualization in wind tunnels using indicators, AGARDograph 70*.

Touré, P. S. R., & Schülein, E. (2020). Scaling for steady and traveling shock wave/turbulent boundary layer interactions. *Exp. Fluids*, *61*(156).

Touré, P. S., & Schülein, E. (2023). Interaction of a moving shock wave with a turbulent boundary layer. *Journal of Fluid Mechanics*, *964*, A28. http://dx.doi.org/10.1017/jfm.2023.357

Wagner, A., Schülein, E., Petervari, R., Hannemann, K., Ali, S. R. C., Cerminara, A., & Sandham, N. D. (2018). Combined free-stream disturbance measurements and receptivity studies in hypersonic wind tunnels by means of a slender wedge probe and direct numerical simulation. *Journal of Fluid Mechanics*, *842*, 495–531. http://dx.doi.org/10.1017/jfm.2018.132